nature communications

Article

https://doi.org/10.1038/s41467-024-51907-4

Plug-and-play protein biosensors using aptamer-regulated in vitro transcription

Received: 18 March 2024

Accepted: 19 August 2024

Published online: 12 September 2024

Check for updates

Heonjoon Lee[1], Tian Xie[2], Byunghwa Kang[3], Xinjie Yu[4], Samuel W. Schaffter[5] & Rebecca Schulman[4,6,7]

Molecular biosensors that accurately measure protein concentrations without external equipment are critical for solving numerous problems in diagnostics and therapeutics. Modularly transducing the binding of protein antibodies, protein switches or aptamers into a useful output remains challenging. Here, we develop a biosensing platform based on aptamer-regulated transcription in which aptamers integrated into transcription templates serve as inputs to molecular circuits that can be programmed to a produce a variety of responses. We modularly design molecular biosensors using this platform by swapping aptamer domains for specific proteins and downstream domains that encode different RNA transcripts. By coupling aptamer-regulated transcription with diverse transduction circuits, we rapidly construct analog protein biosensors and digital protein biosensors with detection ranges that can be tuned over two orders of magnitude and can exceed the binding affinity of the aptamer. Aptamer-regulated transcription is a straightforward and inexpensive approach for constructing programmable protein biosensors that could have diverse applications in research and biotechnology.

Biosensors that detect proteins are crucial for diagnostics[1], smart therapeutics[2], and biomedical research. Traditional ways to detect or measure the concentrations of proteins, such as enzyme-linked immunosorbent assay (ELISA)[3] or Western blot[4] often rely on specific and sensitive binding of antibodies to a target protein. However, these assays are time-consuming and labor-intensive due to multiple incubation and washing steps. Mass spectrometry[5], single-molecule microscopy[6], and electrochemical sensors[7] can detect diverse proteins, but these analytics require expensive and bulky instrumentation, infrastructure, and trained personnel. Further, the output signals of such assays cannot be easily tailored to applications besides protein quantification such as portable diagnostics[8,9] or molecular machines that perform targeted delivery[10,11] in response to disease biomarker detection. Lateral flow assays[12] that rely on antibody binding permit low-cost and rapid detection of proteins, but typically only report the presence of a biomarker and cannot be integrated with downstream reactions that process the input signals[13,14].

Ideally, molecular biosensors could generate a response to a target protein without manual intervention, could be read without specialized equipment, and could easily be programmed to produce a variety of responses. Antibodies[15], protein switches[16], and aptamers[17,18] can be designed to bind to specific proteins, but modularly designing circuits that transduce the protein binding event into a measurable output is challenging. For example, allosteric protein switches[19,20] or aptamers[21–23] that undergo conformational changes upon protein binding to transduce signals have been integrated with molecular circuits. However, designing these structure-switching molecules often requires extensive reengineering for each target protein or desired output[24]. This makes it difficult to rapidly develop protein biosensors against additional targets or to adopt existing biosensors for additional functionalities.

[1]Biomedical Engineering, Johns Hopkins University School of Medicine, Baltimore, MD, USA. [2]Biochemistry and Molecular Biology, Johns Hopkins Bloomberg School of Public Health, Baltimore, MD, USA. [3]Institute for Nanobiotechnology, Johns Hopkins University, Baltimore, MD, USA. [4]Chemical and Biomolecular Engineering, Johns Hopkins University, Baltimore, MD, USA. [5]National Institute of Standards and Technology, Gaithersburg, MD, USA. [6]Computer Science, Johns Hopkins University, Baltimore, MD, USA. [7]Chemistry, Johns Hopkins University, Baltimore, MD, USA. e-mail: samuel.schaffter@nist.gov; rschulm3@jhu.edu

Here, we present aptamer-regulated transcription for in vitro sensing and transduction (ARTIST), which enables rapid construction of protein biosensors that can detect diverse targets and easily integrate with downstream circuits for programmable responses. ARTIST uses aptamer-protein binding to regulate transcription of a DNA template in analogy to the regulation of transcription by protein transcription factor-DNA binding[9,25] (Fig. 1a). Using published DNA aptamer sequences, we show how to simply swap the aptamer domain in these DNA templates for aptamer-regulated transcription (dARTs) to selectively sense a range of proteins, including multiple cytokines involved in autoimmune diseases. Conversely, we modularly swap dART output domains to integrate dARTs with different molecular circuits to create biosensors with different capabilities (Fig. 1b).

Using ARTIST, we build analog biosensors whose outputs indicate protein concentration and digital biosensors in which substantial output is only produced when the protein's concentration exceeds a chosen threshold. The dynamic range of these biosensors can be rationally tuned across multiple orders of magnitude to detect cytokines at physiologically relevant concentrations; even below the aptamer K_d, which often limits biosensor sensitivity in practice. We also demonstrate how ARTIST can be used to create biosensors that are robust to environmental parameters that biosensors are often sensitive to[26], such as ion concentration and enzyme activity. ARTIST is a powerful systems chemistry approach for the facile development of protein biosensors capable of programmable and rapid (<60 min) responses to diverse proteins.

Results

dART design and characterization

The formation of noncanonical DNA structures such as G-quadruplexes have been shown to regulate transcription in cells[27–29] and have been adapted to inhibit in vitro transcription via binding to ions[30] or thrombin[31]. We hypothesized that using this approach[31] we could develop a general protein biosensing platform by designing DNA transcription templates, termed dARTs, with G-quadruplex-forming aptamers downstream of a promoter that repress transcription via protein-aptamer binding. dARTs consist of a promoter domain that T7 RNA polymerase (T7 RNAP) can recognize to initiate transcription, a single-stranded aptamer domain that can bind to a specific protein, and an output domain that T7 RNAP transcribes to produce an RNA output sequence that can react downstream (Fig. 2a).

The aptamer sequence was inserted into the template strand of the dART [30,31], i.e., the strand the polymerase reads during transcription. The output domain of the dART was designed to be double-stranded to prevent spurious interactions between the dART and other species such as the RNA transcribed from the dART, as well as promoter-independent transcription of T7 RNAP (Supplementary Fig. 1). The aptamer and the output sequences are both transcribed from dARTs, so the resulting transcripts could have undesired secondary structure across different input and output sequences (Supplementary Fig. 2, Supplementary Information Note 1.1). To reduce the possibility of such interactions, we added insulation domains, composed of *i* and *i'*, to the dART design (Fig. 2b). The *i* and *i'* domains are complementary and are located on either side of the aptamer sequence so that in the RNA transcript produced from the dART, these domains will hybridize to form a hairpin, sequestering the sequence transcribed from the aptamer domain. (Fig. 2a, Supplementary Information Note 1.2)[32,33]. The *i* domain located just downstream of the promoter was designed to be 6 bases to facilitate efficient T7 RNAP transcription initiation[34] .

We next sought to characterize how our dART design performed in different experimental conditions. For a protein to reduce the rate of dART transcription, the protein must be able to bind to the dART's aptamer and repress transcription, while under the same conditions dARTs should be efficiently transcribed when no protein is present. We began by designing a dART, termed the IFN-O1-dART, that contained an IFN-γ aptamer that forms a G-quadruplex to facilitate IFN-γ binding (Fig. 2c)[35,36]. For characterization, we used a fluorescently labeled DNA reporter complex that reacts with IFN-O1-RNA via toehold-mediated strand displacement (TMSD) to displace one strand of the reporter complex to produce a fluorescent signal (Fig. 2d, "Methods", Supplementary Fig. 3, Supplementary Information Note 1.3).

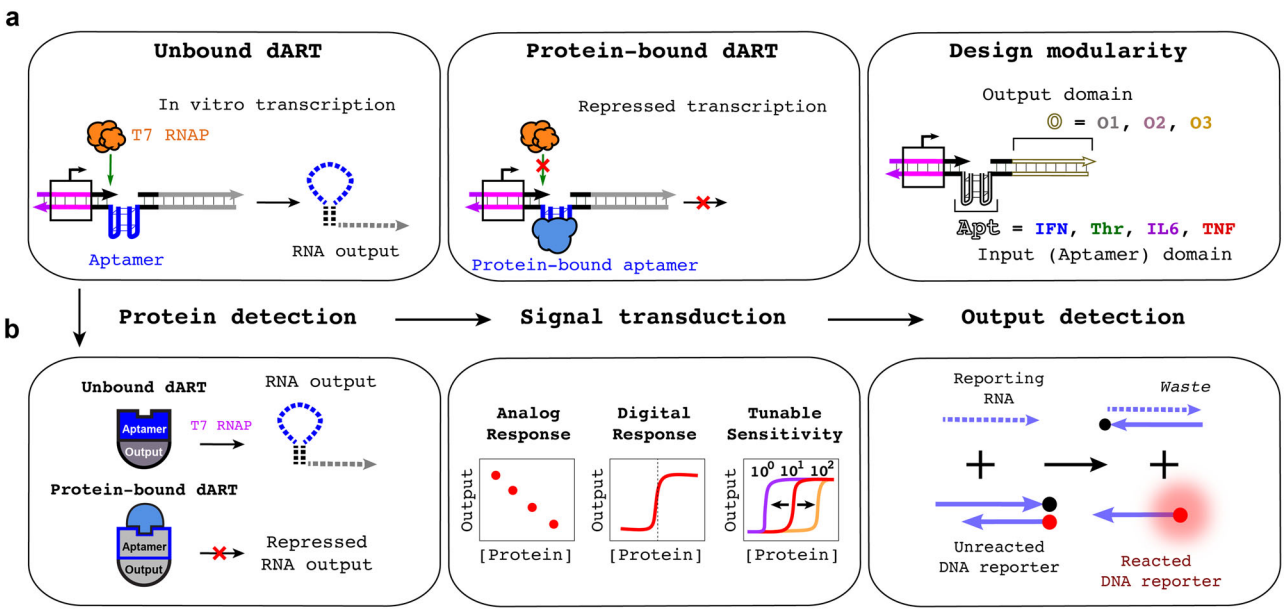

Fig. 1 | The ARTIST platform. a In the absence of an aptamer's protein ligand, dARTs are transcribed to produce an RNA output (left), but protein binding represses transcription (middle). The input and output domains are decoupled (right), which enables modular design of dARTs by swapping out the aptamer domain or customizing the output sequences to encode different RNA outputs. DNA and RNA are represented with solid and dashed lines, respectively. IFN, Thr, IL6, and TNF indicate DNA aptamers for IFN-γ, thrombin, IL-6, and TNF-α, respectively. **b** dARTs serve as the protein sensing layer (left) whose outputs can be coupled with downstream circuits to demonstrate versatile functionalities (middle). The RNA output of molecular circuits can react with a DNA reporter complex (right), which produces measurable fluorescence for detection.

https://doi.org/10.1038/s41467-024-51907-4

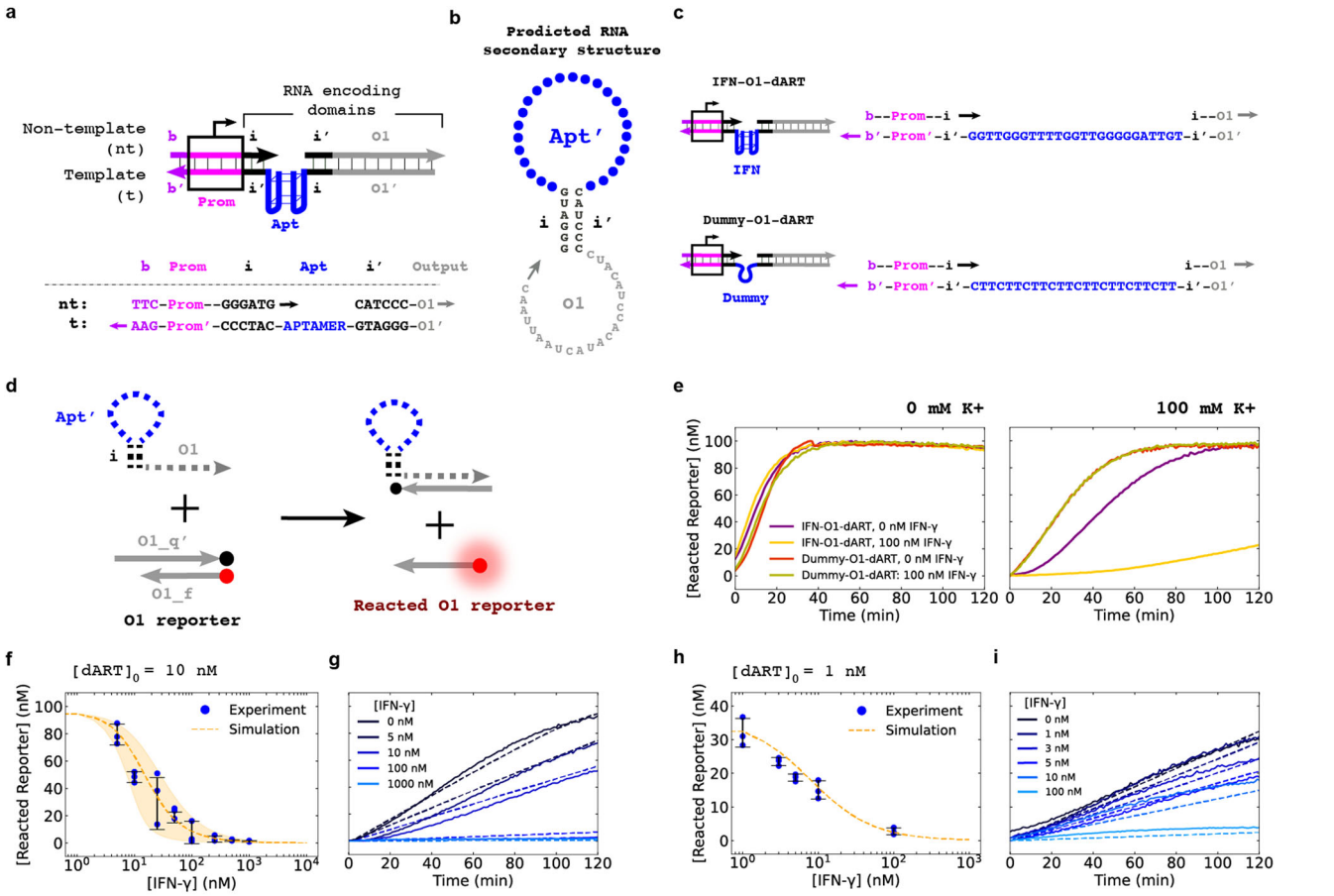

Fig. 2 | Design of aptamer-regulated transcription templates (dARTs). a dART templates consist of a double-stranded promoter region (pink boxed region), a single-stranded aptamer domain on the template strand read by T7 RNAP (Apt), and a double-stranded output domain (O1). The single-stranded aptamer domain permits aptamer-ligand binding. **b** Secondary structure of the RNA transcript predicted by NUPACK[52]. **c** The aptamer sequences of IFN-O1-dART, which binds IFN-γ and Dummy-O1-dART, whose aptamer domain does not have a tertiary structure or specific protein affinity. **d** dART transcripts react with an O1 DNA reporter via toehold-mediated strand displacement. **e** Reacted reporter kinetics from IFN-O1-dART and Dummy-O1-dART transcription with and without IFN-γ and potassium. **f** Simulated and experimental dose–response curves for 10 nM IFN-O1-dART with 0 to 1000 nM IFN-γ for $K_{d,apparent}$ = 8 nM (Supplementary Information Note 2). The dashed line is a simulation for $K_{d,apparent}$ matching experiments. The shaded region shows simulation results for $K_{d,apparent}$ values spanning 1 to 20 nM (see "Methods"). **g** Experimentally measured (bold) and simulated (dashed) reacted reporter kinetics for 10 nM of IFN-O1-dART and 0 to 1000 nM of IFN-γ. **h** Simulated and experimental dose–response curves and **i** Experimental (bold) and simulated (dashed) reacted reporter kinetics (**h**) for 1 nM IFN-O1-dART and 0 to 100 nM of IFN-γ using the $K_{d,apparent}$ determined in (**f**). For (**f**) and (**h**), the reacted reporter concentration for each plot was measured at 120 min. Three technical replicates (blue) are plotted. Error bars indicate the average reacted reporter concentrations of three technical replicates per [IFN-γ] ± one s.d. (N = 3). Supplementary Information Note 2 describes the process for determining $K_{d,apparent}$.

Many G-quadruplex aptamers require potassium ions for effective ligand binding[37,38]. Consistent with this requirement, in the absence of K+, the same rate of fluorescence decrease (i.e., the rate of transcript reaction with the reporter) was observed for IFN-O1-dART in either the presence of 100 nM of IFN-γ or its absence (Fig. 2e), suggesting IFN-γ did not bind to the IFN-O1-dART to reduce transcription rate. When 100 mM KCl was also added, 100 nM IFN-γ was able to substantially repress transcription, consistent with IFN-γ binding to the dART. Without IFN-γ present, the rate of reporter reaction of the IFN-O1-dART was slightly lower with 100 mM of potassium than without potassium, which is consistent with the ability of G-quadruplexes to interrupt transcription[27,30]. In addition, the insulin-linked polymorphic region[39,40] of the human insulin gene was able to fully repress transcription in the presence of 100 mM K+, suggesting that a strong G-quadruplex is sufficient to inhibit transcription in the dART design (Supplementary Supplementary Fig. 4, Supplementary Information Note 1.4)[30,36]. Conversely, a dART with a "dummy" aptamer domain (Dummy-O1-dART), i.e., no specific affinity for IFN-γ and no G-quadruplex forming domain, had similar reacted reporter kinetics for 0 nM or 100 nM of IFN-γ at both 0 mM and 100 mM of K+ (Fig. 2c, e).

As additional controls, we verified that exogenous addition of the same aptamer[36] sequence after 30 min of transcription reversed inhibition of the IFN-O1-dART with 100 nM of IFN-γ (Supplementary Fig. 5). Conversely, adding IFN-γ after 30 min of transcription was able to fully repress transcription with 1000 nM of IFN-γ (Supplementary Fig. 6). We also tested dART variants with i domain lengths ranging from 2 bases to 22 bases (Supplementary Figs. 7, 8, Supplementary Information Note 1.5) and found the 6 base design yielded the greatest difference in transcription rates with and without protein in our experimental conditions (Supplementary Fig. 9).

We next developed a simple model[41] to predict the dose–response and kinetic behavior for 10 nM of IFN-O1-dART incubated with IFN-γ concentrations ranging between 0 and 1000 nM. Our model assumes that transcription cannot occur when a protein is bound to a dART's aptamer, and thus the apparent dissociation constant of the protein and the dART's aptamer, which we termed $K_{d,apparent}$, will dictate the concentration of dART available for transcription at a given protein concentration (Supplementary Information Note 2)[42,43]. This model qualitatively agrees with our measured dose–response curve for a $K_{d,apparent}$ of 8 nM (Fig. 2f and Supplementary Figs. 10–12), which is on

https://doi.org/10.1038/s41467-024-51907-4

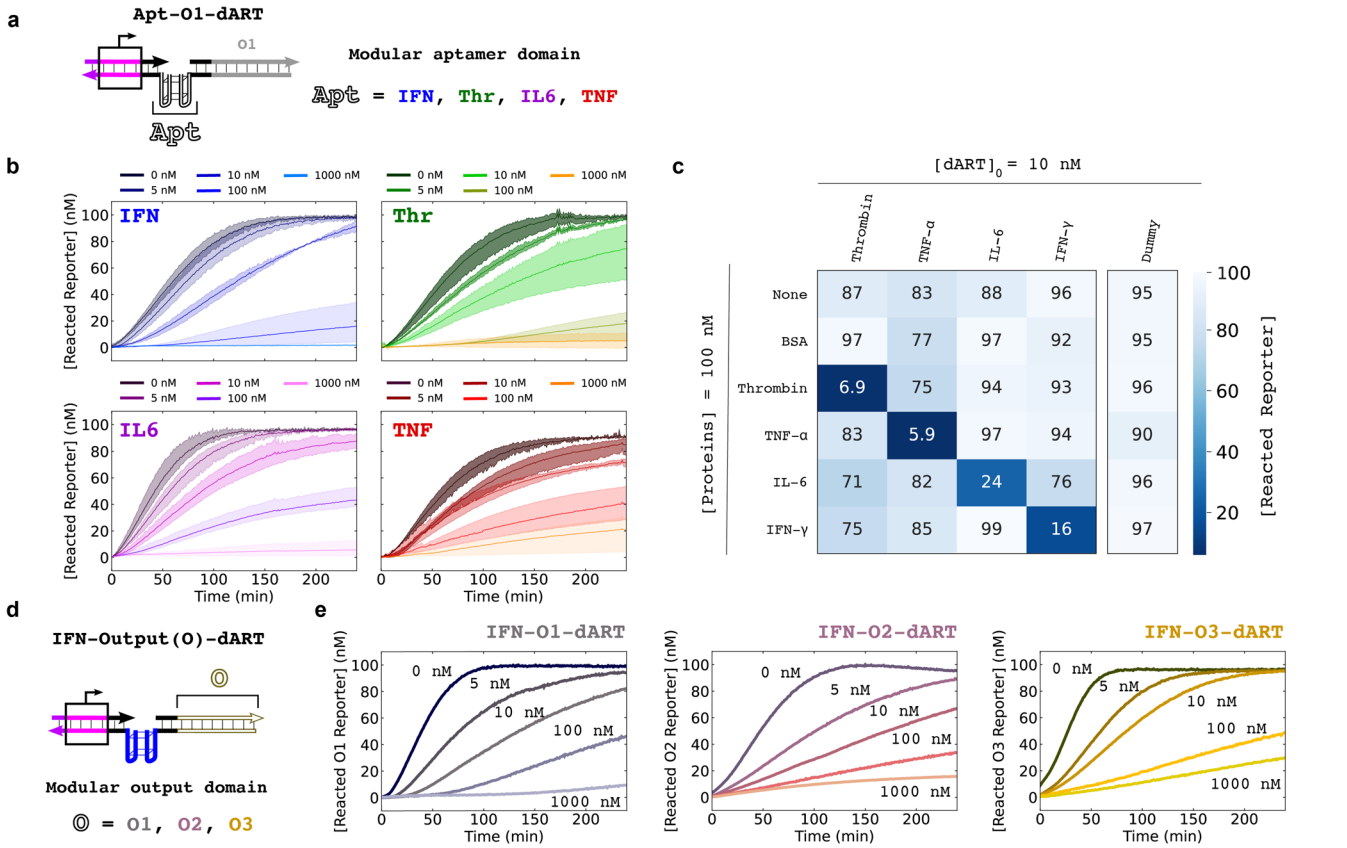

Fig. 3 | dART dose–response, selectivity, and modularity. a A series of dARTs with different inputs, achieved by swapping aptamer domain sequences. **b** Reacted reporter kinetics by IFN-O1-dART, Thr-O1-dART, IL6-O1-dART, and TNF-O1-dART in the presence of 0 to 1000 nM IFN-γ, thrombin, IL-6, and TNF-α, respectively. Shaded regions represent minimum/maximum values of reacted reporter concentration of three replicates ($N = 3$). **c** Heat map showing reacted reporter concentrations for 10 nM Thr-O1-dART, IFN-O1-dART, IL6-O1-dART, TNF-O1-dART, and Dummy-O1-dART (a control) each subjected to 100 nM of BSA, thrombin, TNF-α, IL-6, or IFN-γ. **d** A series of dARTs with different outputs, achieved by swapping template output sequence. **e** Reacted reporter kinetics for IFN-O1-dART, IFN-O2-dART, and IFN-O3-dART for 0 to 1000 nM of IFN-γ. All experiments were conducted in the presence of 100 mM KCl. Sequences of IFN-O1-dART, Thr-O1-dART, IL6-O1-dART, TNF-O1-dART, IFN-O1-dART, IFN-O2-dART, and IFN-O3-dART are in Supplementary Information Note 1.

the same order as the measured K_d of the dART's aptamer sequence[35,36]. Simulations of reacted reporter kinetics were also in good agreement with those measured in experiment (Fig. 2g). Using the model, we then compared the predicted dose–response curve using the $K_{d,apparent}$ of 8 nM to the experimental dose–response curve of 1 nM of IFN-O1-dART in the presence of (0, 1, 3, 5, 10, or 100) nM of IFN-γ. Simulated and experimental results were consistent with each other for both dose–response curve (Fig. 2h) and dose-dependent kinetic profiles (Fig. 2i). Using this model, we estimated the limit of detection[44–46] (LOD) for the 10 nM and 1 nM dARTs to be 6.3 nM (95% CI 3.7–8.9 nM) and 3.7 nM (95% CI 2.0–5.4 nM), respectively (Supplementary Figs. 13 and 14, Supplementary Information Note 3).

We then fit the dose–response curves to a logistic function. Using this fit, the LOD of 10 nM and 1 nM IFN-O1-dART were determined as 4.6 nM (95% CI 2.7–6.5 nM) and 2.0 nM (95% CI 1.0–3.0 nM), respectively, in agreement with the predictions of our kinetic simulations. Based on the slopes of the inflection point of the fit dose–response curves[47,48], the sensitivities of 10 nM and 1 nM IFN-O1-dART were −1.3 (95% CI −0.9–1.7) and −1.2 (95% CI −0.6–1.8), respectively (Supplementary Figs. 13, 14, and 15 Supplementary Information Note 3).

dART input and output modularity

We next asked whether the design of the IFN-O1-dART could be generalized to respond to different protein inputs and produce different RNA outputs. We replaced the IFN-γ aptamer in the IFN-O1-dART with G-quadraplex forming aptamers for thrombin[49], IL-6[50], and TNF-α[51] to create Thr-O1-dART, IL6-O1-dART, and TNF-O1-dART (Fig. 3a, Supplementary Fig. 16, Supplementary Information Note 4.1). NUPACK[52] predicted that the insulation domains would prevent undesired secondary structures from forming in these output RNA sequences (Supplementary Fig. 17).

We measured the reacted reporter kinetics for 10 nM of each of these dARTs when combined with 0 to 1000 nM of their target proteins (Fig. 3b). For all dARTs, the rates of reacted reporter decreased with increasing protein concentrations. We next asked whether these changes in dART reporter reacted were due to specific binding between a target protein and its aptamer. We combined 10 nM of each dART and Dummy-O1-dART with 100 nM of each protein ligand and BSA as a control. Only when dARTs were subjected to their target protein was there a large decrease in the reacted reporter concentration (Fig. 3c and Supplementary Fig. 18). As expected, the dummy template produced a similar concentration of reacted reporter in the presence of all input proteins.

We next asked whether the output domain could also be exchanged modularly, which would allow dARTs to be easily connected to different downstream processes (Fig. 3d, Supplementary Information Note 4.2). We measured transcription profiles of IFN-O1-dART, IFN-O2-dART, and IFN-O3-dART which encode the O1, O2, and O3 output domains, respectively, for 0 to 1000 nM of IFN-γ (Supplementary Figs. 19 and 20). As expected, reacted reporter kinetics decreased with increasing IFN-γ input concentrations for each output (Fig. 3e). This suggests that the outputs of the dARTs could be easily customized to couple them to downstream circuits to create biosensors with different functionalities.

https://doi.org/10.1038/s41467-024-51907-4

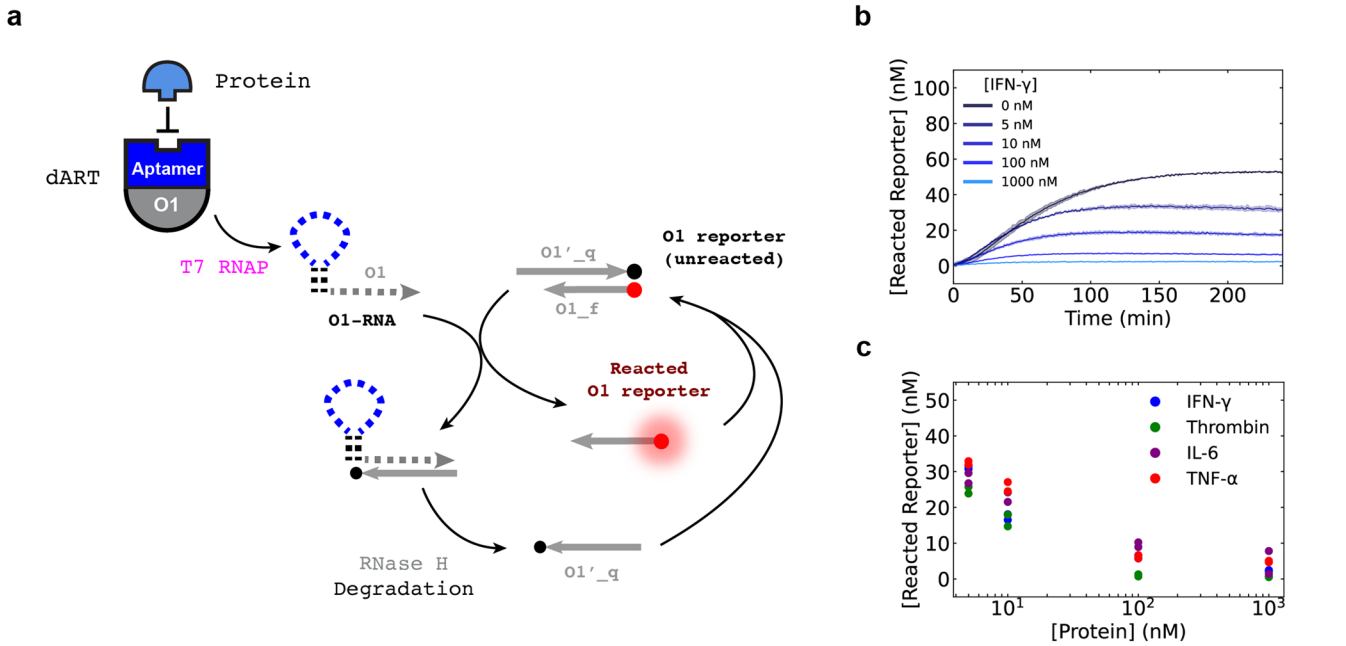

Fig. 4 | Analog biosensors with steady-state outputs. a Schematic of coupled RNA transcription of dARTs by T7 RNAP and RNA degradation by RNase H. **b** The concentration of reacted reporter over time for an experiment with 10 nM IFN-O1-dART, 0 to 1000 nM of IFN-γ, 2 U μL^{-1} of T7 RNAP, and 2×10^{-3} U μL^{-1} of RNase H. Shaded regions enclose the minimum and maximum values for independent trials ($N = 2$; see "Methods"). **c** Steady-state analog outputs of IFN-O1-dART, Thr-O1-dART, IL6-O1-dART, and TNF-O1-dART with 5 to 1000 nM of their corresponding proteins after 240 min. Two individual technical replicates are plotted ($N = 2$).

Not all aptamer sequences we pulled from the literature worked in dARTs. For example, we tested four aptamer sequences for VEGF[53] (Supplementary Figs. 21 and 22, Supplementary Information Note 4.3), and observed that one had the desired response (Supplementary Figs. 23 and 24). The other three sequences showed repressed transcription with potassium even without VEGF. Thus, these aptamer sequences may form stable enough G-quadruplexes with K+ alone to repress transcription. Alternatively, modeling of the secondary structure of the outputs of the poor performing dARTs suggested that some of the transcripts may adopt undesigned secondary structures that impedes their ability to react with their reporters (Supplementary Fig. 21). These results suggest a simple screening protocol for adopting additional aptamer sequences to ARTIST by measuring transcription of dARTs with and without potassium prior to testing with ligand.

Analog biosensors

We next asked whether we could use ARTIST to build biosensors with different functionalities, such as analog or digital response, or signal amplification by coupling dARTs to downstream reactions. In principle, the rate of increase of reacted reporter by a dART is a measure of the target protein's concentration. However, rates are difficult to measure because they require observing a signal over time. We thus asked whether we might build analog biosensors that indicate protein concentration as the steady-state concentration of reacted reporter by adding RNase H. RNase H degrades RNA outputs of a dART bound to the DNA strand O1'_q[32,54], allowing O1'_q to rehybridize to O1_f to reform the quenched reporter complex after degradation (Fig. 4a). A balance of RNA production and degradation should therefore produce a steady-state response whose magnitude is dependent on the concentration of the target protein. The reacted reporter concentrations of IFN-O1-dART with 0 to 1000 nM of IFN-γ indeed reached different steady-state values for different input protein concentrations in the presence of RNase H (Fig. 4b, c). When Thr-O1-dART, IL6-O1-dART, and TNF-O1-dART were combined with reporter and 5 to 1000 nM of their corresponding input proteins, distinct steady-state reacted reporter concentrations were also observed after 240 min (Supplementary Information Note 5, Supplementary Fig. 25, Fig. 4c).

Digital biosensors

We next asked how we might use ARTIST to construct digital biosensors that have a high sensitivity across a threshold concentration i.e., they produce a high output signal when the input exceeds the threshold concentration and a low output signal otherwise. Digital biosensors are also important for measuring whether a sample satisfies a specific diagnostic criterion. We sought to design digital biosensors that invert the output signal of individual dARTs, so that a high protein concentration yields a high concentration of RNA output. We designed a digital biosensor for IFN-γ by integrating two dARTs to produce a comparator circuit. A reference dART with an aptamer domain that does not bind IFN-γ was designed to produce the O1 output (Ref-O1-dART). Another dART with the IFN-γ aptamer domain was designed to produce an output with partial complementarity to the O1 sequence (IFN-O1'-dART) (Fig. 5a, Supplementary Information Note 6.1, Supplementary Fig. 26). If the IFN-O1'-dART is added at a higher concentration than the Ref-O1-dART, then IFN-O1'-RNA will sequester Ref-O1-RNA, resulting in a low reporter signal in the absence of protein. As IFN-γ concentration is increased, the rate of IFN-O1'-RNA transcription will decrease, allowing the Ref-O1-RNA to react with the O1 reporter once a threshold IFN-γ concentration is reached (Fig. 5b). This comparator circuit also inverts.

We first sought to build a comparator circuit that could threshold the concentration of IFN-γ so that [IFN-γ] < 20 nM would produce a low reacted reporter signal (OFF) and [IFN-γ] ≥ 50 nM would produce a high signal (ON). We used simulations with the previously measured $K_{d,apparent}$ for the IFN-O1-dART (Supplementary Information Note 6.2, 6.3, and 6.4, Supplementary Fig. 27) to determine that 25 nM of Ref-O1-dART and 50 nM of IFN-O1'-dART should produce a digital response with the desired threshold (Supplementary Fig. 28 and Fig. 5c). These predictions were then confirmed in experiments (Fig. 5d, e). We termed this IFN-γ O1 comparator circuit involving 25 nM of Ref-O1-dART and 50 nM of IFN-O1'-dART, IFN-C-50-O1. Compared to 10 nM of

https://doi.org/10.1038/s41467-024-51907-4

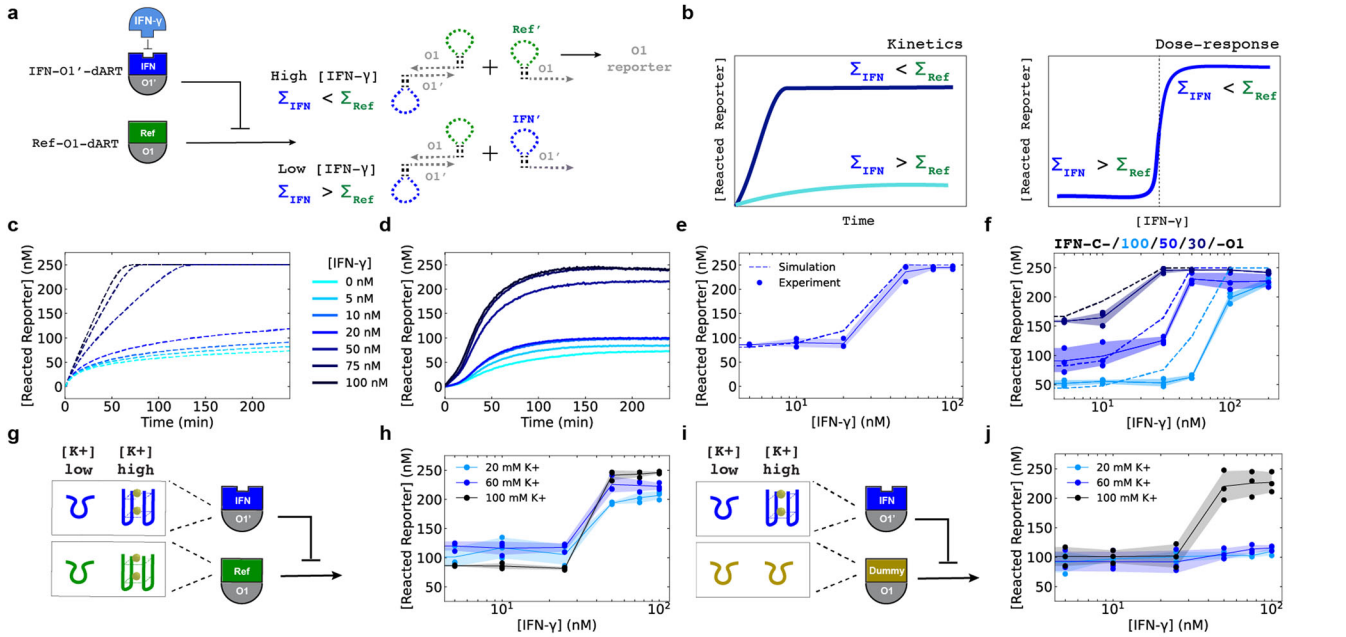

Fig. 5 | Comparator circuits for digital biosensing. a The comparator circuit. When [IFN-γ] is high, IFN-O1′-dART's transcription rate is low. Ref-O1-RNA is thus produced in excess, and it reacts with the O1 DNA reporter. When [IFN-γ] is low, IFN-O1′-RNA's transcription rate is higher than Ref-O1-RNA's, and Ref-O1-RNA is sequestered by IFN-O1′-RNA before it can react with the reporter. **b** Illustrations of desired responses of the digital biosensor. Left: when [IFN-γ] is high, reacted reporter rises concentration should increase rapidly until all reporter is reacted, When [IFN-γ] is low it should rise slowly or not at all. Right: the concentration of reacted reporter should therefore either be fully ON or very low (OFF) at the end of the reaction. **c** Simulated kinetics of IFN-C-50-O1. **d** Experimentally measured kinetics of IFN-C-50-O1. **e** Dose–response curve of IFN-C-50-O1 after 240 min of reaction. Dashed lines represent simulations, whereas the points represent experimental values. **f** The dose–response curves of IFN-C-30-O1, IFN-C-50-O1, and IFN-C-100-O1. **g** The comparator is designed to be K+-insensitive. IFN-O1′-dART and Ref-O1-dART both form G-quadruplexes, and their transcription rates should change similarly with [K+] concentrations so the output of the comparator should be relatively insensitive to [K+]. **h** Dose–response curves of IFN-C-50-O1 in (**g**); responses were measured after 240 min. The line plots are added to aid visualization of the trends in the reacted reporter concentrations for each [K+] concentration. **i** A [K+]-sensitive comparator. At high [K+], the aptamer domain on the IFN-O1′-dART forms a G-quadruplex, which reduces its transcription rate. If the IFN-O1′-dART's output is compared to an RNA produced at a rate insensitive to [K+] (from Dummy-O1-dART) output should change with [K+]. **j** Dose–response curves of IFN-C-50-O1 with Dummy-O1-dART for different [K+]; responses were measured after 240 min. The line plots are added to aid visualization of the trends for each [K+] concentration. For (**e**), (**f**), (**h**), and (**j**), three individual technical replicates are plotted. Lines connect the average reacted reporter concentrations of three technical replicates per [IFN-γ]. Shaded regions indicate ± one s.d. ($N = 3$). See Supplementary Information Note 6.2, 6.3, and 6.4 for simulation equations and parameters.

IFN-O1-dART, the digital IFN-C-50-O1 biosensor exhibited a 5-fold increase in sensitivity across the threshold concentration (Supplementary Fig. 15, Supplementary Information Note 3).

We reasoned we could tune the IFN-γ threshold of IFN-C-50-O1 by changing the concentration of Ref-O1-dART, which would change the amount of IFN-O1′-dART that must be repressed by input protein to produce a reporter signal (Supplementary Information Note 6.4)[13]. In line with this intuition, we found that an IFN-γ O1 comparator circuit with 15 nM of Ref-O1-dART required ≥100 nM IFN-γ to turn on (IFN-C-100-O1), while a circuit with 40 nM Ref-O1-dART only required ≥30 nM IFN-γ to turn on (IFN-C-30-O1; Fig. 5f).

Robust digital responses

We hypothesized that the digital response of IFN-C-50-O1 would also be insensitive to different environmental factors that often affect biosensors. For example, T7 RNAP activity can vary with solution composition[55] or temperature[56], and such variations could lead to false positives or false negatives. Since a comparator computes the ratio of the transcription rates of a dART and a reference template, its output should not change substantially with T7 RNAP activity, because changes in T7 RNAP activity would alter the transcription rates of both templates in the same way. Indeed, the IFN-C-50-O1 produced low reacted reporter concentrations for [IFN-γ] <20 nM and high reacted reporter concentrations for [IFN-γ] ≥ 50 nM, when T7 RNAP activities were either 2, 4, or 8 U μl^{-1} (Supplementary Figs. 29 and 30, Supplementary Information Note 6.5).

Different biological samples contain a wide range of potassium ion concentrations such as blood (3.5–5 mM)[57], saliva (20–22 mM)[58], and urine (40–100 mM)[59]. The affinity of G-quadruplex-forming aptamers for their ligands is also sensitive to potassium[37,60,61], meaning that affinity assays involving these aptamers would have different performance in these different media. Consistent with this finding, dART transcription rate decreased with increasing potassium concentration (Supplementary Information Note 6.6, Supplementary Fig. 31). However, both dARTs comprising IFN-C-50 contain G-quadraplexes (Fig. 5g), so their transcription rates are affected in similar ways by different potassium concentrations. As a result, IFN-C-50-O1 had similar digital responses and response thresholds across different potassium concentrations (Fig. 5h). In contrast, a comparator with a reference dART with a dummy aptamer sequence (Fig. 2c, Supplementary Table 1) that does not form a G-quadruplex (Fig. 5i), becomes non-responsive at lower potassium ions concentrations (Fig. 5j, Supplementary Fig. 31) because the IFN-O1′-dART transcription rate changes with potassium concentration, but the Dummy-O1-dART transcription rate does not, changing the threshold. Another challenge to the use of ARTIST for biological samples is the presence of RNases in most samples. Compared to our conventional dART assay conditions, we found IFN-C-50-O1 had a similar sensitivity in 10 (v/v)% serum supplemented with RNase inhibitor (Supplementary Fig. 33)[23,62]. We also confirmed that IFN-C-50-O1 triggered at the designed IFN-γ threshold concentration in 10 (v/v)% supernatant from cultures of Chinese hamster ovary (CHO) cells that were secreting VRC01

https://doi.org/10.1038/s41467-024-51907-4

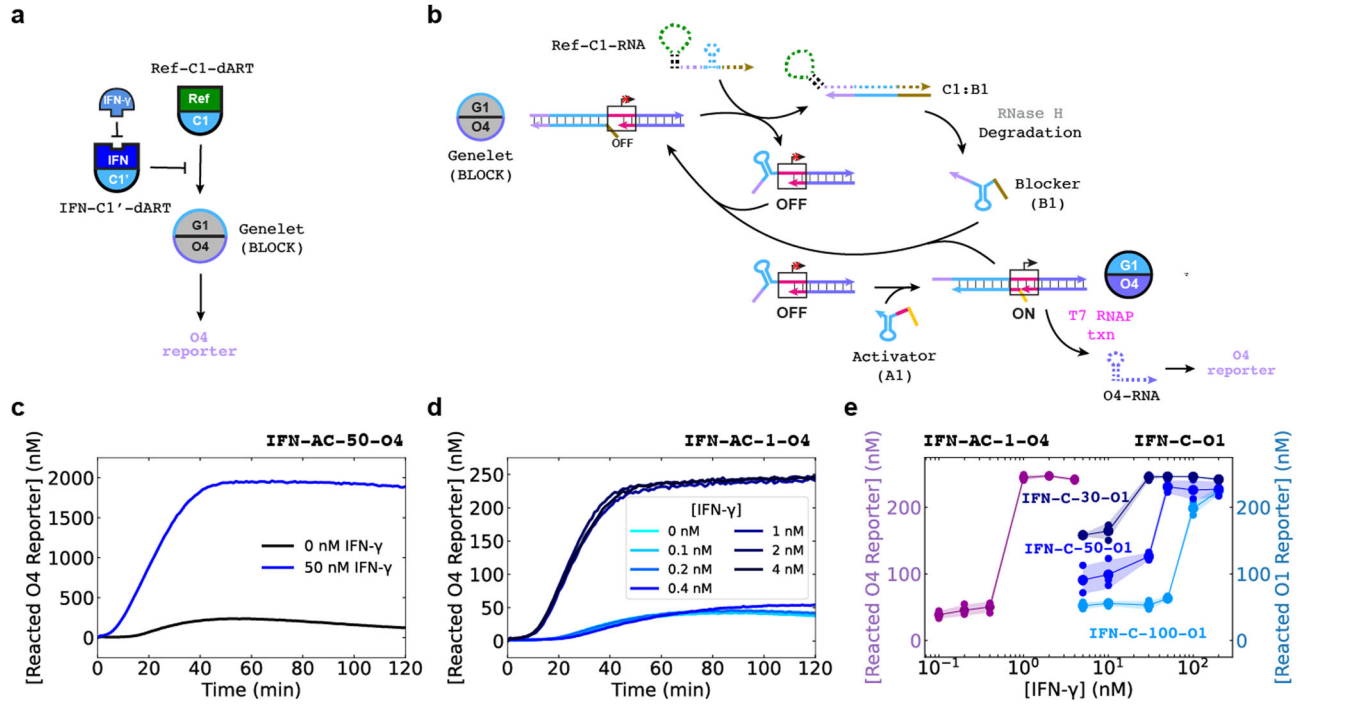

Fig. 6 | Sensitive protein detection with amplified comparators. a Circuit diagram for an amplified IFN-C1′-dART/Ref-C1-dART comparator. The Ref-C1-RNA output, which is high when IFN-γ exceeds a threshold concentration, activates transcription of a genelet that transcribes O4, which is detected by a reporter. **b** The reactions through which Ref-C1-RNA coactivates G1O4 to produce the O4 output. **c** Reacted reporter kinetics of IFN-AC-50-O4, which consists of 25 nM Ref-C1-dART, 50 nM IFN-C1′-dART, 100 nM G1O4:B1, 200 nM A1, and 2000 nM O4 DNA reporter, for 0 nM or 50 nM IFN-γ. **d** Reacted reporter kinetics of the IFN-AC-1-O4, which consists of 0.5 nM of Ref-C1-dART, 1 nM IFN-C1′-dART, 20 nM of G1O4:B1, and 100 nM of A1, and 250 nM of O4 DNA reporter for IFN-γ inputs from 0 to 4 nM. 4 U μL^{-1} T7 RNAP and 4×10^{-3} U μL^{-1} RNase H were used in IFN-AC-1-O4. **e** Comparison of the dose–response curves of IFN-AC-1-O4, IFN-C-30-O1, IFN-C-50-O1, and IFN-C-100-O1. Three individual technical replicates are plotted. Lines connect the average reacted reporter concentrations of three technical replicates per [IFN-γ]. Shaded regions indicate the average value of three technical replicates ± one s.d. ($N = 3$).

monoclonal antibodies (Supplementary Fig. 34). These results show how ARTIST could be used to construct digital biosensors that reliably detect proteins under different environmental conditions.

Output amplification

We next asked whether we might increase the amount of output produced by a comparator circuit in response to the same concentrations of protein input. We designed an amplified comparator (Fig. 6a, Supplementary Information Note 7) in which the RNA output of the comparator circuit activates transcription of a downstream genelet[32] via strand displacement reactions that complete the promoter sequence of the genelet (Fig. 6b, Supplementary Figs. 35 and 36). To prevent the low level of comparator output that is produced even when [IFN-γ] is low from triggering the output, we included RNase H, so that only when the rate of Ref-C1-RNA production exceeds its degradation rate can it activate the genelet to produce an output.

The amplified comparator (IFN-AC-50-O4) reacted with 2000 nM of O4 reporter (Fig. 6c) in response to 50 nM of IFN-γ in <45 min, more than 40 times the output produced by the non-amplified comparator to the same input (IFN-C-50-O4; Supplementary Fig. 37). Without IFN-γ, about 200 nM of O4 reporter reacted transiently, but this amount then decreased, presumably because of RNase H-catalyzed O4 RNA degradation. Interestingly, the ON/OFF ratio of IFN-C-50-O4 was only 2-fold to 3-fold (Supplementary Fig. 37), compared to IFN-AC-50-O4, which was nearly 10-fold (Fig. 6c). This increase in the fold-change between the ON and OFF signals may be due to two factors. First, Ref-O1-RNA reacts faster with the O1 reporter in IFN-C-50-O1 than Ref-C1-RNA does with B1 in IFN-AC-50-O4[32]. Thus, when IFN-C1′-RNA is in excess, a greater fraction of Ref-C1-RNA is sequestered in IFN-C-50-O4 than IFN-O4-RNA in IFN-C-50-O4. Second, in IFN-AC-50-O4, both Ref-C1-RNA and O4-RNA are degraded by RNase H, which results in a lower background signal without protein for IFN-AC-50-O4 than for IFN-C-50-O4.

We hypothesized that an amplified comparator such as IFN-AC-50-O4 could be tuned to produce a similar amount of high output to its corresponding non-amplified comparator (IFN-C-50-O4) beginning above a much lower threshold protein concentration. To build this more sensitive amplified comparator, we reduced the concentrations of the Ref-C1-dART and IFN-C1′-dART of IFN-AC-50-O4 50-fold to create a diluted amplified comparator, termed IFN-AC-1-O4. IFN-AC-1-O4 maximized reporter signal for IFN-γ concentrations of 1 nM or higher and otherwise produced <12% of the maximum reporter signal. Amplifying the output of the comparator thus makes it possible to reduce the threshold input concentration of the circuit 50-fold (Supplementary Fig. 38), decrease the limit of detection below 1 nM, and maintain high sensitivity (Fig. 6d, e, Supplementary Fig. 15, Supplementary Information Note 3). Furthermore, the concentration of reacted reporter, a measure of the RNA output, produced by IFN-AC-1-O4 at this threshold is >250-fold higher than the input protein concentration (Fig. 6d, e).

Discussion

ARTIST is a versatile platform for rapidly developing biosensors that report on protein concentrations. By coupling downstream reactions to a dART's protein-controlled transcription processes, ARTIST can be easily tailored to produce biosensors with analog responses, tunable digital responses, and high sensitivities below the K_d of an aptamer.

ARTIST's performance suggests it could be used for sensing proteins of interest in research and clinical settings. For example, IFN-γ is a ubiquitous cytokine involved in various malignancies (e.g., cancer, autoimmune diseases)[63], as well as a key signalling factor in immunotherapy. T-cells can secret up to 30 nM of IFN-γ during mitogenic

stimulation[64] and activated lymphocytes can secrete up to 3.5 nM of IFN-γ after transfection of immunotherapies[65]. The ARTIST biosensors presented here are already suited to detect proteins within these biologically relevant ranges, with the IFN-C-30-O1 and IFN-AC-1-O4 biosensors designed to respond at 8.7 nM and 0.4 nM of IFN-γ, respectively. Incorporating additional layers of genelet amplification[66] or other isothermal RNA amplification schemes that have been able to detect femtomolar concentrations of nucleic acids[67] could enable ARTIST biosensors that respond well below the current LOD of 0.4 nM[66,67].

Aptamers identified in previous studies were readily integrated into dARTs, suggesting the promise of developing a larger library of biosensors for a range of important protein targets. The selectivity of dARTs suggests that they may be combined to allow for multiplexed sensing or decision-making involving multiple protein inputs. They could also be integrated with methods such as proximity ligation[68] or multi-epitope targeting[69] to enhance selectivity for detection in more complex environments. G-quadruplex-forming aptamers, which have been developed for more than 2000 proteins[70], were investigated here, but non-G-quadruplex-forming sequences have also been reported to repress in vitro transcription[30], suggesting that ARTIST may apply to an even broader range of aptamers.

It should be possible to incorporate ARTIST into existing field-deployable workflows for rapid point-of-need biosensing. The constituents of ARTIST (T7 RNAP, RNase H, DNA complexes) can be easily freeze-dried for storage and the outputs are compatible with existing portable systems to measure fluorescence[8,9]. Testing in matrices such as serum, blood, urine, and saliva can severely inhibit reaction conditions, and will need to be systematically studied. Our results in serum and supernatant from antibody secreting CHO cell cultures indicate RNase inhibitors can help with operating biosensors within biological samples by preventing RNA degradation[23,62].

The effects of environmental conditions such as ion concentration on aptamer affinity can limit their applicability in biosensors. We demonstrate how the ARTIST system can produce a measurement of IFN-γ concentration that is mostly insensitive to that concentration of potassium ions, despite the effects of potassium on aptamer affinity[38]. Biological samples such as serum, blood, urine, and saliva, have different salt concentrations that can confound the readout of biosensors. ARTIST, through the ability to self-calibrate in response to its environment, may potentially ameliorate this issue. The incorporation of further self-calibration, background, or crosstalk subtraction[71] or even feedback control methods such as adaptation[72] might allow ARTIST to overcome many of these limitations, or further, even to achieve robustness levels exceeding those of many traditional affinity assays.

Methods

Materials

O4_f, O1'_q, O2'_q, O3'_q, and O4'_q were purchased from Integrated DNA Technologies (IDT) with HPLC purification (Supplementary Table 1). All other oligonucleotides were purchased under standard desalting conditions. Triphosphates (NTPs) were purchased from ThermoFisher Scientific (R0481). T7 RNAP was purchased in bulk (300,000 U) from Cellscript (200 U μl^{-1}, C-T7300K) as well as from ThermoFisher Scientific (200 U μl^{-1}, EP0113). NEB RNAPol reaction buffer (M0251S; 10X) and yeast inorganic pyrophosphatase (YIPP; M2403S; 0.1 U μl^{-1}) were purchased from New England Biolabs (NEB). RNase H was purchased from ThermoFisher Scientific (EN0201; 5 U μl^{-1}). Fetal bovine serum (FBS; 26140079) and RNase inhibitor (N8080119; 0.5 U μl^{-1}) were purchased from ThermoFisher Scientific. CHOZN cell line (Sigma-Aldrich) expressing the VRC01 monoclonal antibody was cultured in imMEDIAte Advantage Medium (Catalog No. 87093C; Millipore-Sigma-Aldrich) in batch mode. The suspension cells were cultured in 125 ml shake flask with working volume of 30 ml at 125 RPM, 37 °C, and 5% carbon dioxide. Cells were inoculated at 5.0×10^5 cells mL^{-1}. Culture media supernatants were collected after 4 days of culture.

Recombinant Human IFN-γ (285-IF), IL-6 (206-IL), TNF-α (210-TA), and VEGF 165 (293-VE) were all purchased from R&D Systems Inc. (USA) in lyophilized form. Recombinant Human IFN-γ was reconstituted in sterile, deionized water, whereas Recombinant Human IL-6, TNF-α, and VEGF were all reconstituted in sterile PBS containing 0.1% BSA. Human α-thrombin (HCT0020) was purchased from Haematologic Technologies, Inc. (Essex, VT) and dissolved in 50% H_2O/glycerol.

dART annealing and preparation

dARTs were assembled by annealing their three strands, a promoter non-template strand (Prom-dART-nt), a non-template strand encoding the output sequence of choice (i.e., O1-dART-nt, O2-dART-nt, O3-dART-nt) and a template strand that contains the aptamer domain of choice that is complementary to the two non-template strands (i.e., IFN-O1-dART-t, Thr-O1-dART-t, IL6-O1-dART-t, TNF-O1-dART-t) at equimolar concentrations. As an example, Prom-dART-nt, O1-dART-nt, and IFN-O1-dART-t were combined in a standard 200 μL PCR tube (VMR; 20170-010) at concentrations of 1 μM per strand in 1X NEB RNAPol reaction buffer supplemented with KCl to a final concentration of 100 mM. To anneal, mixtures were heated to 90 °C, incubated for 5 min, then cooled to 20 °C at a rate of 1 °C min^{-1}.

Reporter annealing and preparation

DNA reporters were prepared by diluting the fluorophore-modified DNA strand with its partially complementary quencher-modified DNA strand at a concentration of 10 μM per strand in 1X NEB RNAPol reaction buffer. The reporter mixture was heated to 90 °C, incubated for 5 min, then cooled to 20 °C at a rate of 1 °C min^{-1}.

Amplified comparator annealing and preparation

Genelet initially in a blocked state (G1O4:B1) was prepared by mixing G1O4-nt, O4-t, and B1 together in 1X NEB RNAPol reaction buffer at equimolar concentrations. The genelet mixture was heated to 90 °C, incubated for 5 min, then cooled to 20 °C at a rate of 1 °C min^{-1}.

Reaction conditions

Reactions were all conducted at 37 °C in 1X NEB RNAPol reaction buffer supplemented with KCl to a final concentration of 100 mM and NTPs (ATP, UTP, CTP, GTP) at a final concentration of 2 mM each unless otherwise stated. We included 100 mM KCl to promote the proper folding of G-quadruplex structures within aptamer domains[27]. In addition to T7 RNA polymerase, YIPP was also included in reactions (1.35×10^{-3} U μl^{-1}) to extend the duration of the transcription reactions. The reaction conditions mentioned above are referred to as ARTIST reaction conditions. The concentrations of each of the molecules in each experiment are given in Supplementary Tables 10–31 under Supplementary Information Note 8. The total volume of the reaction was set at 25 μL for all assays.

To perform experiments, solutions containing dART templates under ARTIST reaction condition mentioned were first added to wells of a 384-well plate. Proteins were then added at the concentrations described set at a volume of 0.5 μL and in most experiments incubated for 30 min to 60 min at room temperature. In Supplementary Fig. 6, IFN-γ was added after 30 min of transcription to measure repression of IFN-O1-dART. In Fig. 3b, we also added 0.5 μL of sterile PBS containing 0.1% BSA into the assays with 10 nM of IL6-O1-dART or TNF-O1-dART reacting with 0 nM of IL-6 or TNF-α, respectively. This was done to ensure equal salt concentrations from the PBS buffer. Similarly in Supplementary Fig. 15, we added 0.5 μL of sterile PBS containing 0.1% BSA into all assays that did not have 100 nM of IL-6 or TNF-α. IFN-C-O1-50 was mixed in 10 (v/v)% FBS (Supplementary Fig. 33) or 10 (v/v)% CHO cell culture media (Supplementary Fig. 34), and 0 to 100 nM of IFN-γ. The reaction mix was incubated

with 0.5 U μL^{-1} of RNase inhibitor for 2 h before adding in T7 RNAP and YIPP.

Data acquisition

Fluorescence readings were then taken for 10 min to 25 mins to measure minimum fluorescence values before T7 RNAP, and YIPP were added to initiate the reactions (Supplementary Information Note 1.2, Supplementary Fig. 3a). At the end of the experiments, 0.5 μL of a DNA strand fully complementary to o1'_q or o4'_q was mixed into each assay at a final concentration of 2.5 μM to obtain a maximum O1 or O4 DNA reporter fluorescence intensity. Fluorescence data were then normalized using Eq. 1 as follows (Supplementary Fig. 3b):

$$[\text{Reacted Reporter}] = (\text{Total}\,[\text{DNA Reporter}]) * \frac{\text{Fluorescence} - \text{Min}\,(\text{Fluorescence})}{\text{Max}\,(\text{Fluorescence}) - \text{Min}\,(\text{Fluorescence})} \quad (1)$$

All kinetic data were obtained using either a BioTek Synergy H1 or Cytation 5 plate reader (Agilent Technologies). All fluorescence readings were measured using Gen5 3.11 (BioTek Synergy H1) and 3.12 (Cytation 5). HEX was measured with an excitation peak of 533 nm and an emission peak of 559 nm with a gain of 80 to 100 to ensure fluorescence values were within the linear range of detection. Cy3 was measured with excitation peak of 555 nm and emission peak of 569 nm with a gain 60 to 100 to ensure fluorescence values were within the linear range of detection. FAM was measured with excitation peak of 487 nm and emission peak of 527 nm with a gain of 60. Fluorescence measurements were taken every minute during reactions.

Data analysis

Determination of standard deviations for all data points shown in Supplementary Figs. 13, 14, and 15 were determined from the covariance estimates using SciPy's curvefit function.

Statistics and reproducibility

For technical replicates, all experiments were conducted using the same instrument, reagents, and experimental conditions on two or three separate days. Error bars and shadings indicate ± one s.d. Randomization is not relevant to our study. Under Supplementary Note 3, the 95% confidence intervals of EC_{50} and p parameters were determined from the covariance estimates supplied by SciPy's curvefit function.

Reporting summary

Further information on research design is available in the Nature Portfolio Reporting Summary linked to this article.

Data availability

All data generated in this study are provided in the Supplementary Information and Source data file. Source data are provided with this paper.

Code availability

All data analysis, simulations for $K_{d,apparent}$, reacted reporter kinetics of dARTs, reacted reporter kinetics, dose–response curves of the comparator, and LogFit analysis of sensitivity and LOD are available at: https://doi.org/10.7281/T1/IRL0IE[41].

References

1. Soper, S. A. et al. Point-of-care biosensor systems for cancer diagnostics/prognostics. *Biosens. Bioelectron.* **21**, 1932–1942 (2006).
2. Shen, L., Wang, P. & Ke, Y. DNA nanotechnology-based biosensors and therapeutics. *Adv. Health. Mater.* **10**, 2002205 (2021).
3. Rissin, D. M. et al. Single-molecule enzyme-linked immunosorbent assay detects serum proteins at subfemtomolar concentrations. *Nat. Biotechnol.* **28**, 595–599 (2010).
4. Rivero-Gutiérrez, B., Anzola, A., Martínez-Augustin, O. & de Medina, F. S. Stain-free detection as loading control alternative to Ponceau and housekeeping protein immunodetection in Western blotting. *Anal. Biochem.* **467**, 1–3 (2014).
5. Jannetto, P. J. & Fitzgerald, R. L. Effective use of mass spectrometry in the clinical laboratory. *Clin. Chem.* **62**, 92–98 (2016).
6. Orrit, M., Ha, T. & Sandoghdar, V. Single-molecule optical spectroscopy. *Chem. Soc. Rev.* **43**, 973 (2014).
7. Wu, J., Liu, H., Chen, W., Ma, B. & Ju, H. Device integration of electrochemical biosensors. *Nat. Rev. Bioeng.* **1**, 346–360 (2023).
8. Pardee, K. et al. Paper-based synthetic gene networks. *Cell* **159**, 940–954 (2014).
9. Jung, J. K. et al. Cell-free biosensors for rapid detection of water contaminants. *Nat. Biotechnol.* **38**, 1451–1459 (2020).
10. Sedlmayer, F., Aubel, D. & Fussenegger, M. Synthetic gene circuits for the detection, elimination and prevention of disease. *Nat. Biomed. Eng.* **2**, 399–415 (2018).
11. Douglas, S. M., Bachelet, I. & Church, G. M. A logic-gated nanorobot for targeted transport of molecular payloads. *Science (1979)* **335**, 831–834 (2012).
12. Bahadır, E. B. & Sezgintürk, M. K. Lateral flow assays: principles, designs and labels. *TrAC Trends Anal. Chem.* **82**, 286–306 (2016).
13. Jung, J. K., Archuleta, C. M., Alam, K. K. & Lucks, J. B. Programming cell-free biosensors with DNA strand displacement circuits. *Nat. Chem. Biol.* **18**, 385–393 (2022).
14. Ma, Q. et al. An automated DNA computing platform for rapid etiological diagnostics. *Sci. Adv.* **8**, eade0453 (2022).
15. Ni, Y. et al. A plug-and-play platform of ratiometric bioluminescent sensors for homogeneous immunoassays. *Nat. Commun.* **12**, 4586 (2021).
16. Choi, J. H., Laurent, A. H., Hilser, V. J. & Ostermeier, M. Design of protein switches based on an ensemble model of allostery. *Nat. Commun.* **6**, 6968 (2015).
17. Tuerk, C. & Gold, L. Systematic evolution of ligands by exponential enrichment: RNA ligands to bacteriophage T4 DNA polymerase. *Science* **249**, 505–510 (1990).
18. Ellington, A. D. & Szostak, J. W. In vitro selection of RNA molecules that bind specific ligands. *Nature* **346**, 818–822 (1990).
19. Ribeiro, L. F., Warren, T. D. & Ostermeier, M. Construction of protein switches by domain insertion and directed evolution. 43–55. https://doi.org/10.1007/978-1-4939-6940-1_3 (2017).
20. Quijano-Rubio, A. et al. De novo design of modular and tunable protein biosensors. *Nature* **591**, 482–487 (2021).
21. Simmel, F. C., Yurke, B. & Singh, H. R. Principles and applications of nucleic acid strand displacement reactions. *Chem. Rev.* **119**, 6326–6369 (2019).
22. Oh, S. S., Plakos, K., Lou, X., Xiao, Y. & Soh, H. T. In vitro selection of structure-switching, self-reporting aptamers. *Proc. Natl Acad. Sci.* **107**, 14053–14058 (2010).
23. Vezeau, G. E., Gadila, L. R. & Salis, H. M. Automated design of protein-binding riboswitches for sensing human biomarkers in a cell-free expression system. *Nat. Commun.* **14**, 2416 (2023).
24. Stein, V. & Alexandrov, K. Synthetic protein switches: design principles and applications. *Trends Biotechnol.* **33**, 101–110 (2015).
25. van der Meer, J. R. & Belkin, S. Where microbiology meets microengineering: design and applications of reporter bacteria. *Nat. Rev. Microbiol.* **8**, 511–522 (2010).
26. Boyd, M. A., Thavarajah, W., Lucks, J. B. & Kamat, N. P. Robust and tunable performance of a cell-free biosensor encapsulated in lipid vesicles. *Sci. Adv.* **9**, (2023).

27. Broxson, C., Beckett, J. & Tornaletti, S. Transcription arrest by a G quadruplex forming-trinucleotide repeat sequence from the human c-myb gene. *Biochemistry* **50**, 4162–4172 (2011).
28. Bochman, M. L., Paeschke, K. & Zakian, V. A. DNA secondary structures: stability and function of G-quadruplex structures. *Nat. Rev. Genet* **13**, 770–780 (2012).
29. Lee, C.-Y. et al. R-loop induced G-quadruplex in non-template promotes transcription by successive R-loop formation. *Nat. Commun.* **11**, 3392 (2020).
30. Zhang, P. et al. Topologically switchable and gated transcription machinery. *Chem. Sci.* **13**, 10555–10565 (2022).
31. Iyer, S. & Doktycz, M. J. Thrombin-mediated transcriptional regulation using DNA aptamers in DNA-based cell-free protein synthesis. *ACS Synth. Biol.* **3**, 340–346 (2014).
32. Schaffter, S. W. et al. Standardized excitable elements for scalable engineering of far-from-equilibrium chemical networks. *Nat. Chem.* **14**, 1224–1232 (2022).
33. Bhadra, S. & Ellington, A. D. Design and application of cotranscriptional non-enzymatic RNA circuits and signal transducers. *Nucleic Acids Res.* **42**, e58–e58 (2014).
34. Conrad, T., Plumbom, I., Alcobendas, M., Vidal, R. & Sauer, S. Maximizing transcription of nucleic acids with efficient T7 promoters. *Commun. Biol.* **3**, 439 (2020).
35. Kimoto, M., Yamashige, R., Matsunaga, K., Yokoyama, S. & Hirao, I. Generation of high-affinity DNA aptamers using an expanded genetic alphabet. *Nat. Biotechnol.* **31**, 453–457 (2013).
36. Hashim, S. N., Tsuchiya, A., Kamiya, N. & Sando, S. A single fluorophore-labeled aptamer sensor for the detection of interferon gamma. *Chem. Lett.* **44**, 1670–1672 (2015).
37. Bhattacharyya, D., Mirihana Arachchilage, G. & Basu, S. Metal cations in G-quadruplex folding and stability. *Front. Chem.* **4**, 38 (2016).
38. Dong, J., O'Hagan, M. P. & Willner, I. Switchable and dynamic G-quadruplexes and their applications. *Chem. Soc. Rev.* **51**, 7631–7661 (2022).
39. Lew, A., Rutter, W. J. & Kennedy, G. C. Unusual DNA structure of the diabetes susceptibility locus *IDDM2* and its effect on transcription by the insulin promoter factor Pur-1/MAZ. *Proc. Natl Acad. Sci. USA* **97**, 12508–12512 (2000).
40. Connor, A. C., Frederick, K. A., Morgan, E. J. & McGown, L. B. Insulin capture by an insulin-linked polymorphic region G-quadruplex DNA oligonucleotide. *J. Am. Chem. Soc.* **128**, 4986–4991 (2006).
41. Lee, H. et al. Data associated with the publication: Plug-and-play protein biosensors using aptamer-regulated in vitro transcription. https://doi.org/10.7281/T1/IRL0IE, Johns Hopkins Research Data Repository, V1 (2024).
42. Maganzini, N., Thompson, I., Wilson, B. & Soh, H. T. Pre-equilibrium biosensors as an approach towards rapid and continuous molecular measurements. *Nat. Commun.* **13**, 7072 (2022).
43. Jarmoskaite, I., AlSadhan, I., Vaidyanathan, P. P. & Herschlag, D. How to measure and evaluate binding affinities. *Elife* **9**, e57264 (2020).
44. De Acha, N., Socorro-Leránoz, A. B., Elosúa, C. & Matías, I. R. Trends in the design of intensity-based optical fiber biosensors (2010–2020). *Biosensors* **11**, 197 (2021).
45. Shrivastava, A. & Gupta, V. Methods for the determination of limit of detection and limit of quantitation of the analytical methods. *Chron. Young. Sci.* **2**, 21 (2011).
46. Mann, M. M. & Berger, B. W. A genetically-encoded biosensor for direct detection of perfluorooctanoic acid. *Sci. Rep.* **13**, 15186 (2023).
47. Yu, J., Zhang, Y., Zhao, Y., Zhang, X. & Ren, H. Highly sensitive and selective detection of inorganic phosphates in the water environment by biosensors based on bioluminescence resonance energy transfer. *Anal. Chem.* **95**, 4904–4913 (2023).
48. Swank, Z., Laohakunakorn, N. & Maerkl, S. J. Cell-free gene-regulatory network engineering with synthetic transcription factors. *Proc. Natl Acad. Sci.* **116**, 5892–5901 (2019).
49. Tasset, D. M., Kubik, M. F. & Steiner, W. Oligonucleotide inhibitors of human thrombin that bind distinct epitopes. *J. Mol. Biol.* **272**, 688–698 (1997).
50. Spiridonova, V. A., Novikova, T. M. & Snigirev, O. V. Obtaining DNA aptamers to human interleukin-6 for biomagnetic immunoassay nanosensors. *Mosc. Univ. Phys. Bull.* **71**, 135–138 (2016).
51. Orava, E. W., Jarvik, N., Shek, Y. L., Sidhu, S. S. & Gariépy, J. A short DNA aptamer that recognizes TNFα and blocks its activity in vitro. *ACS Chem. Biol.* **8**, 170–178 (2013).
52. Zadeh, J. N. et al. NUPACK: analysis and design of nucleic acid systems. *J. Comput. Chem.* **32**, 170–173 (2011).
53. Nonaka, Y. et al. Affinity Improvement of a VEGF Aptamer by in Silico Maturation for a Sensitive VEGF-Detection System. *Anal. Chem.* **85**, 1132–1137 (2013).
54. Del Grosso, E., Franco, E., Prins, L. J. & Ricci, F. Dissipative DNA nanotechnology. *Nat. Chem.* **14**, 600–613 (2022).
55. Borkotoky, S. & Murali, A. The highly efficient T7 RNA polymerase: a wonder macromolecule in biological realm. *Int J. Biol. Macromol.* **118**, 49–56 (2018).
56. Chamberlin, M. & Ring, J. Characterization of T7-specific ribonucleic acid polymerase. *J. Biol. Chem.* **248**, 2235–2244 (1973).
57. Nakhoul, G. N. et al. Serum potassium, end-stage renal disease and mortality in chronic kidney disease. *Am. J. Nephrol.* **41**, 456–463 (2015).
58. Aps, J. K. M. & Martens, L. C. Review: The physiology of saliva and transfer of drugs into saliva. *Forensic Sci. Int.* **150**, 119–131 (2005).
59. Maciel, A. T., Vitorio, D. & Osawa, E. A. Urine biochemistry assessment in the sequential evaluation of renal function: Time to think outside the box. *Front. Med.* **9**, 912877 (2022).
60. Ogasawara, S. Transcription driven by reversible photocontrol of hyperstable G-quadruplexes. *ACS Synth. Biol.* **7**, 2507–2513 (2018).
61. Russo Krauss, I. et al. High-resolution structures of two complexes between thrombin and thrombin-binding aptamer shed light on the role of cations in the aptamer inhibitory activity. *Nucleic Acids Res.* **40**, 8119–8128 (2012).
62. Soltani, M. & Bundy, B. C. Streamlining cell-free protein synthesis biosensors for use in human fluids: In situ RNase inhibitor production during extract preparation. *Biochem Eng. J.* **177**, 108158 (2022).
63. Gocher, A. M., Workman, C. J. & Vignali, D. A. A. Interferon-γ: teammate or opponent in the tumour microenvironment? *Nat. Rev. Immunol.* **22**, 158–172 (2022).
64. Zhu, H. et al. Detecting cytokine release from single T-cells. *Anal. Chem.* **81**, 8150–8156 (2009).
65. Tzeng, S. Y. et al. In situ genetic engineering of tumors for long-lasting and systemic immunotherapy. *Proc. Natl Acad. Sci. USA* **117**, 4043–4052 (2020).
66. Wan, X. et al. Cascaded amplifying circuits enable ultrasensitive cellular sensors for toxic metals. *Nat. Chem. Biol.* **15**, 540–548 (2019).
67. Pardee, K. et al. Rapid, low-cost detection of Zika virus using programmable biomolecular components. *Cell* **165**, 1255–1266 (2016).
68. Fredriksson, S. et al. Protein detection using proximity-dependent DNA ligation assays. *Nat. Biotechnol.* **20**, 473–477 (2002).
69. Chang, X. et al. Construction of a multiple-aptamer-based DNA logic device on live cell membranes via associative toehold activation for accurate cancer cell identification. *J. Am. Chem. Soc.* **141**, 12738–12743 (2019).
70. Shahsavar, K., Hosseini, M., Shokri, E. & Xu, G. New insight into G-quadruplexes; diagnosis application in cancer. *Anal. Biochem.* **620**, 114149 (2021).
71. Müller, I. E. et al. Gene networks that compensate for crosstalk with crosstalk. *Nat. Commun.* **10**, 4028 (2019).

72. Frei, T. & Khammash, M. Adaptive circuits in synthetic biology. *Curr. Opin. Syst. Biol.* **28**, 100399 (2021).

Acknowledgements

The authors thank Michael Betenbaugh and Junneng Wen for providing the CHO cell culture media, as well as Marc Ostermeier, Elizabeth Strychalski, Simon d'Oelsnitz, Moshe Rubanov, Everett Kengmana, Colin Yancey, and Lei Zhang for insightful conversations and comments on the manuscript. H.L. was supported by the Asan Foundation Biomedical Science Scholarship. S.W.S. was supported by a National Research Council Postdoctoral Fellowship. R.S. acknowledges support from NIH R21CA251027-01A1, NSF CIF Medium 2107246, and ARO award W911NF2010057 and ARL award W911NF2220246. The National Institute of Standards and Technology notes that certain commercial equipment, instruments, and materials are identified in this paper to specify an experimental procedure as completely as possible. In no case does the identification of particular equipment or materials imply a recommendation or endorsement by NIST, nor does it imply that the materials, instruments, or equipment are necessarily the best available for the purpose.

Author contributions

H.L., S.W.S., and R.S. designed the research. H.L. conducted most of the experiments and simulations. T.X. performed some experiments in Figs. 2f, h, and 3b of the main text and Supplementary Fig. 9 under Supplementary Information. X.Y. performed some experiments for Fig. 3e. H.L., B.K., and R.S. conducted simulations and analysis to estimate the LODs of dARTs in Supplementary Information Note 3. H.L., B.K., S.W.S., and R.S. wrote the paper with feedback from the other authors.

Competing interests

H.L., B.K., S.W.S., and R.S. are co-inventors of a pending patent application (WO/2024/118806). The remaining authors declare no competing interests.

Additional information

Supplementary information The online version contains supplementary material available at https://doi.org/10.1038/s41467-024-51907-4.

Correspondence and requests for materials should be addressed to Samuel W. Schaffter or Rebecca Schulman.

Peer review information *Nature Communications* thanks the anonymous reviewers for their contribution to the peer review of this work. A peer review file is available.

Reprints and permissions information is available at http://www.nature.com/reprints

Publisher's note Springer Nature remains neutral with regard to jurisdictional claims in published maps and institutional affiliations.

Open Access This article is licensed under a Creative Commons Attribution-NonCommercial-NoDerivatives 4.0 International License, which permits any non-commercial use, sharing, distribution and reproduction in any medium or format, as long as you give appropriate credit to the original author(s) and the source, provide a link to the Creative Commons licence, and indicate if you modified the licensed material. You do not have permission under this licence to share adapted material derived from this article or parts of it. The images or other third party material in this article are included in the article's Creative Commons licence, unless indicated otherwise in a credit line to the material. If material is not included in the article's Creative Commons licence and your intended use is not permitted by statutory regulation or exceeds the permitted use, you will need to obtain permission directly from the copyright holder. To view a copy of this licence, visit http://creativecommons.org/licenses/by-nc-nd/4.0/.

© The Author(s) 2024